THE JOURNAL OF PHYSICAL CHEMISTRY C

Article

pubs.acs.org/JPCC

The Interaction of Cobalt with CeO_2(111) Prepared on Cu(111)

Gábor Vári,[†] László Óvári,*[,‡] Christian Papp,[§] Hans-Peter Steinrück,[§] János Kiss,[‡] and Zoltán Kónya[†,‡]

[†]Department of Applied and Environmental Chemistry, University of Szeged, H-6720 Szeged, Rerrich Béla tér 1, Hungary

[‡]MTA-SZTE Reaction Kinetics and Surface Chemistry Research Group, H-6720 Szeged, Rerrich Béla tér 1, Hungary

[§]Chair of Physical Chemistry II, University of Erlangen-Nürnberg, Egerlandstr. 3, 91058 Erlangen, Germany

ABSTRACT: The interaction of cobalt with an ultrathin CeO_2(111) film on Cu(111) was studied by low energy ion scattering spectroscopy and X-ray photoelectron spectroscopy. At room temperature, Co grows three-dimensionally on the ceria film. For small Co coverages (0.2 ML), oxidation to Co^{2+} occurs together with the formation of Ce^{3+} in the ceria. At higher Co coverages (0.7 and 2 ML), an increasing fraction of Co remained metallic after deposition. Annealing to higher temperatures induced diffusion of Co^{2+} ions into the ceria film, and for metallic Co, presumably agglomeration occurs. At $T \geq 800$ K, oxidation of significant amounts of Co^0 to Co^{2+} is found, along with diffusion into the ceria film, and partly also in the copper crystal underneath. On a reduced CeO_x surface, the redox reaction between cobalt and cerium was hindered, which, in turn, slowed down cobalt migration into the ceria film.

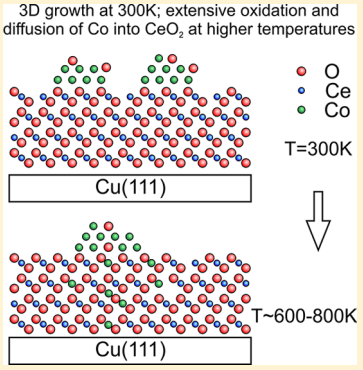

1. INTRODUCTION

Ceria is a key component in a number of catalyst formulations designed for applications in the environment and energy sector. These applications benefit from the outstanding redox properties of ceria, which are, in turn, associated with the surface properties as well as the shape and dimensions of its crystals.[1,2] Ceria-supported precious metal catalysts such as Rh, Pd, and Pt are widely used in many important applications, including three-way automobile emission-control catalysis, water gas shift reactions, fuel cells, and also hydrogen production from ethanol; this versatility is due to the peculiar redox properties and oxygen storage capacity of ceria as well as the synergetic effect between metals and the ceria support.[1−10]

However, the prices of these metals are very high. As an alternative, the less expensive transition metal Co is considered to be a promising catalyst for certain reactions, for example, as a mixed oxide, in CO oxidation[11] and also for steam reforming of ethanol (SRE). Indeed, Co promotes the C−C bond rupture in adsorbed ethanol. It achieves high ethanol conversion and selectivities to H_2 and CO_2 on CeO_2, and on other supports, even at relatively low temperatures (~723 K).[12−16] Recent studies suggested that Co^{2+} sites or partially oxidized Co particles are the active centers in SRE, and pure metallic Co^0 patches are responsible for coke formation.[17,18] In contrast, other authors considered metallic cobalt to play the key role in SRE.[19]

In order to obtain a deeper understanding of the relevant surface processes during these complicated catalytic reactions, it is useful to construct simplified, but well controlled, experimental model systems. One established approach is using oxide single crystals or single crystalline oxide films, and preparing nanoclusters of the active metal on top.[20−25] The low conductivity of CeO_2 single crystals (e.g., compared to that of TiO_2) motivated intense research activities aiming at the preparation of ultrathin single crystalline CeO_2 films on various metallic supports, such as Ru(0001),[26,27] Cu(111),[28−34] and Pd(111).[35] The most frequently applied recipe for the preparation of continuous CeO_2(111) layers on Cu(111) is the deposition of Ce in an O_2 background of ~5×10^{-7} mbar at 523 K at a rate of 0.08−0.15 ML/min. 1 ML of CeO_2(111) layer is defined as one O-Ce-O trilayer of the fluorite structure of bulk CeO_2 (3.13 Å, 7.87×10^{14} Ce atoms/cm^2).[36] This method, which yields well ordered, but not atomically smooth, CeO_2(111) films with a (1.5 × 1.5) superstructure on Cu(111),[29−32] was applied in the present work. The films are kinetically stabilized, since there is general agreement that the CeO_2(111)/Cu(111) system thermodynamically follows the Volmer−Weber (three-dimensional island) growth mode, probably due to the weak interaction between the oxide and the support.[31,32,34] In a previous paper, we investigated the effect of oxygen pressure on ceria growth at 523 K.[34] Our low energy ion scattering (LEIS) and X-ray photoelectron spectroscopy (XPS) data indicate that the increase in the oxygen pressure from 5×10^{-7} to 3×10^{-6} mbar leads to a slightly more oxidized ceria layer; at the same time, a significant part of copper atoms were oxidized to Cu^{1+}, possibly incorporated in the CeO_2 film. Moreover, the continuity of the film was somewhat worse; i.e., wetting was less pronounced.[34]

The exploration of the interaction between Co and CeO_2(111) is fundamental to understand surface chemical reactions on this supported catalytic system. The growth of Co on CeO_2(111) was briefly studied previously using XPS: On

Received: January 21, 2015
Revised: April 2, 2015
Published: April 3, 2015

DOI: 10.1021/acs.jpcc.5b00626
J. Phys. Chem. C 2015, 119, 9324−9333

the basis of the linear dependence of the Ce 3d/Co 2p area ratio on cobalt coverage, a two-dimensional (2D) growth of Co was proposed up to 1 ML.[37] From the Co 2p peak shape, the resulting surface species were identified as Co^0 and Co^{2+}. Furthermore, reduction of Ce was observed upon Co deposition, due to the reaction of Co with CeO_2.[7,37] The ratio of Co^{2+} to Co^0 decreased with increasing Co coverage. The increase of the Ce(3d)/Co(2p) ratio upon annealing was attributed to a partial agglomeration of the Co film to form particles.[37]

The interaction of other metals with $CeO_2(111)$ was also investigated previously. Rh and Pd formed 3D nanoparticles at 300 K, and STM revealed agglomeration upon annealing.[38] Similarly, a Volmer−Weber growth mode was identified by STM for gold deposition on $CeO_2(111)$ films, with most of the Au particles formed at the step edges and at defect sites on terraces.[39]

The growth of cobalt was studied also on other oxides. On the basis of the coverage dependence of Zn/Co XPS and AES signal ratios, an approximate layer-by-layer growth mode was assumed on ZnO(0001) at 300 K, although with some 3D character as well. A metallic oxidation state prevailed upon Co deposition. Annealing induced mostly agglomeration up to 700 K, followed by oxidation of Co and spreading on ZnO up to 800 K, and the diffusion of Co into ZnO at 850−900 K.[40] Dumont et al. reported island growth applying STM, while annealing led to the diffusion of Co into ZnO.[41] A 3D growth mode of Co was identified on alumina prepared on NiAl(110).[42] The Co deposits prepared by PVD on nearly stoichiometric $TiO_2(110)$ were dominated by the metallic component at 300 K, and no thermal induced redox reaction was identified by XPS between TiO_2 and Co upon annealing. However, the strong attenuation of Co 2p features at 900 K was attributed to the diffusion of Co into titania.[43]

In the present study, we determine the growth mode of cobalt on $CeO_2(111)$ by LEIS. This method is particularly suited for that purpose, since it is almost exclusively sensitive to the outermost atomic layer.[44] Therefore, in the case of a layer-by-layer growth, the complete suppression of substrate signal is expected upon the completion of the first layer, while the changes are much smaller for XPS. Our results point toward a Volmer−Weber growth mode for Co on $CeO_2(111)$. Additionally, we also address the thermal evolution of the cobalt−ceria interaction for stoichiometric and reduced $CeO_2(111)$ films using XPS and LEIS. While the redox reaction between Co and nearly stoichiometric ceria (at 300 K) presented in this paper is rather similar to that described by Martono et al.,[37] herein it is complemented by the study of the same process on reduced ceria and also by the investigation of thermally induced changes in the oxidation states. Regarding morphology, our results indicate the diffusion of cobalt into ceria at higher temperatures.

2. EXPERIMENTAL SECTION

The experiments were carried out in a UHV chamber with a base pressure of 5×10^{-10} mbar. It is equipped with a Leybold hemispherical analyzer for performing LEIS, XPS, and Auger electron spectroscopy measurements, and with a quadrupole mass spectrometer for residual gas analysis. A SPECS IQE 12/38 ion source was used for LEIS. He^+ or Ne^+ ions with 800 eV kinetic energy were applied at a low ion flux of ~0.03 $\mu A/cm^2$. The incident and detection angles were 50° with respect to the surface normal, while the scattering angle was 95°. The angle between the "incident plane" (the plane defined by the ion source axis and the surface normal) and the "detection plane" (the plane defined by the surface normal and the analyzer axis) was 53°. An Al Kα X-ray source was applied for XPS. The binding energy scale was calibrated against the $4f_{7/2}$ peak of a thick Au layer (84.0 eV) and the $2p_{3/2}$ peak of the clean Cu(111) surface (932.6 eV). XPS was performed with a constant pass energy, and with a detection angle of 16° (off normal). Peak fitting of the Ce 3d XPS region and of the LEIS spectra obtained with helium was executed using Gaussian−Lorentzian line shapes and Shirley baselines.[45] Asymmetric peaks were allowed for LEIS. All spectra are presented without smoothing.

The Cu(111) single crystal was a product of MaTeck (purity: 99.9999%; orientation accuracy: 0.1°). It was heated radiatively with a W filament from behind. The temperature was measured by a chromel−alumel (K-type) thermocouple inserted into a hole in the crystal. The surface was routinely cleaned applying cycles of Ar^+ ion sputtering (10 $\mu A/cm^2$, 1.5 keV) at 300 K and vacuum annealing (5 min, 1000 K).

The purity of O_2 (Linde) was 99.995%. Ce (99.9%) and Co (99.99%) were deposited by a commercial 4-pocket PVD source (Oxford Applied Research). The Co coverage was defined to be 1 ML, if the surface concentration of Co atoms was equal to the surface concentration of Co atoms on the Co(0001) surface (1.8×10^{15} atoms/cm^2). The Ce and Co fluxes were checked by a quartz crystal microbalance (QCM). $CeO_2(111)$ was deposited at a sample temperature of 523 K, evaporating Ce at a rate of 0.07 ML/min in 5×10^{-7} mbar of O_2. At the end of preparation, O_2 was pumped down at $T = 400$ K.

3. RESULTS AND DISCUSSION

3.1. Cobalt Growth on $CeO_2(111)$ at 300 K. The information depth of LEIS with noble gas ions is restricted to the outermost atomic layer due to the dominance of single scattering. Thereby, the impinging noble gas ions are directly scattered off one surface atom toward the analyzer, and almost all noble gas ions participating in multiple collisions are neutralized and consequently cannot be detected.[44] Since neutralization is significant also for single scattering events, the intensity of an ion scattering peak depends sensitively on the neutralization probability of the impinging noble gas ions upon the collision with the surface atoms.[44] Although matrix effects for the neutralization probability (i.e., changes in the neutralization during scattering from a given atom as a function of its chemical environment), sometimes simply referred to as "neutralization effects", are relatively rare in LEIS, these can severely hinder a quantitative evaluation of the data, if they arise.[44] Previous LEIS studies of metallic and oxidized cerium deposits on other metallic substrates reported serious difficulties related to the neutralization of noble gas ions.[35,46] For this reason, we specifically addressed possible neutralization effects related to the growth of Ce and CeO_2 on Cu(111) in a preceding paper.[34] The conclusions most relevant for the present study are (i) for metallic Ce, no neutralization effects were found with He^+, but such effects were detected with Ne^+. Interestingly, they only affect the neutralization of Ne^+ ions on Ce, but not on Cu; therefore, the Cu(Ne) peak can still be used for quantitative analysis. (ii) No neutralization effects were observed for CeO_2 on Cu(111) with He^+ and with Ne^+. The relative sensitivity factors obtained (separately) for the binary Cu−O and Cu−Ce systems using He^+ could be applied also for

DOI: 10.1021/acs.jpcc.5b00626
J. Phys. Chem. C 2015, 119, 9324−9333

the ternary Cu−Ce−O system. The $CeO_2(111)$ film is assumed to be oxygen-terminated. Nevertheless, since the O ions of the outermost oxygen layer are rather loosely packed,[47] with a lattice constant of 3.826 Å, and since the outermost Ce layer is only slightly below the O plane (by 0.78 Å), this Ce layer also contributes to the LEIS spectra.

In the present work, we first investigated the deposition of Co on a 16 ML thick $CeO_2(111)$ film near room temperature with LEIS (Figure 1). As expected, with increasing Co coverage, a diminution of the Ce peak was observed with both He^+ and Ne^+. The LEIS spectra obtained with He^+ and Ne^+ clearly indicate that the deposition of nominally 1 ML of Co (blue spectrum) does not lead to the complete suppression of the Ce peak: it was detected even at Θ_{Co} = 8 ML (orange spectrum in Figure 1b), which unequivocally indicates that Co on ceria does not grow in a layer-by-layer fashion. This conclusion is different from what was suggested by other authors based on XPS results.[37] It should be mentioned that LEIS is better suited to the identification of the growth mode than XPS, because of its topmost layer sensitivity. The observed behavior can be explained either by growth in three-dimensional (3D) islands (Volmer−Weber type growth) or by a mixing of Co and Ce atoms/ions already at room temperature. The inspection of the LEIS peak areas as a function of Co coverage reveals some further details of Co growth (Figure 2).

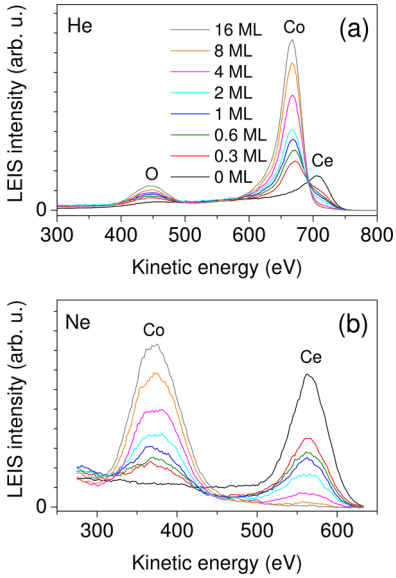

Figure 1. LEIS spectra obtained with He^+ (a) and Ne^+ (b), after the deposition of increasing amounts of Co on 16 ML $CeO_2(111)$/Cu(111) at 320 K.

For Co/Ce intermixing upon cobalt deposition, one would expect that the mixing is more efficient initially, that is, at the Co−CeO_2 interface, while it should be less probable at later stages of the growth, when the Co atoms landing on the surface of a cobalt deposit are farther away from the interface. This behavior would lead to a milder attenuation of the Ce LEIS peak at small Co coverages, and a steeper one at larger coverages. However, if 3D island growth occurs, then a steeper decrease in the Ce peak would be expected at small coverages, because very small metal clusters are often two-dimensional. The growth mode can change to three-dimensional at higher coverages, resulting in a slower attenuation of the substrate

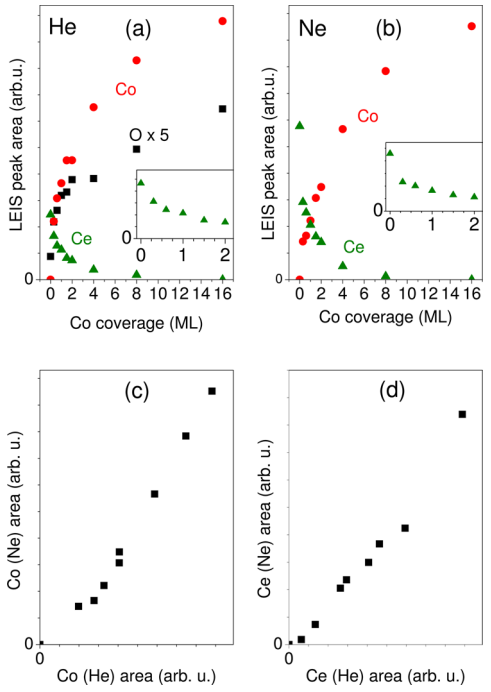

Figure 2. LEIS peak areas obtained with helium (a) and neon (b) during stepwise deposition of Co on 16 ML $CeO_2(111)$/Cu(111) at 320 K. The insets show the decrease in the Ce (He) and Ce (Ne) areas at smaller Co coverages. (c) The Co peak area detected with Ne^+ as a function of the Co area obtained with He^+. (d) The Ce peak area detected with Ne^+ as a function of the Ce area obtained with He^+.

peak. In fact, while both Au and Rh follow 3D island growth on $TiO_2(110)$, at small, submonolayer coverages, (quasi) two-dimensional clusters form.[23,48] In our case, the decrease in the Ce(He) and Ce(Ne) LEIS areas is less steep at higher Co coverages, clearly indicating that the growth occurs in 3D islands. The deposition of 1 ML of Co resulted in a 54% and 64% decrease in the Ce(He) and Ce(Ne) areas, respectively. Nevertheless, at small coverages (up to 0.3 ML), the steep attenuation of Ce LEIS areas might indicate an approximate 2D character. Accordingly, the dependence of the substrate Ce LEIS areas on the admetal Co coverage is very similar to what was observed for other Volmer−Weber systems, like Rh, Au, and Pt on $TiO_2(110)$.[23,48,49] Nevertheless, a small contribution of mixing of Ce and Co to the observed changes cannot be excluded.

We also checked for possible neutralization effects in the Co−CeO_2 system. If there are no neutralization matrix effects for a system consisting of elements A and B, then, upon changing the surface composition, the LEIS peak area for A (I_A) is a linear function of that for B (I_B), if the geometrical shadowing effect of a deposited atom does not change with coverage. This characteristic behavior is widely used to check for the absence of neutralization effects.[44,50] Such a linear relationship demonstrated that no neutralization effects occur for the Cu−O system in our previous study.[34] For the deposition of metallic Ce on Cu(111), the linearity of the I_{Cu}(He) vs I_{Ce}(He) curve confirmed the absence of matrix effects with He^+, but the I_{Cu}(Ne) vs I_{Ce}(Ne) curve was nonlinear.

As pointed out in ref 34, further information can be gathered from the inspection of the peak areas obtained with neon as a function of the peak areas detected with helium: If in a binary

DOI: 10.1021/acs.jpcc.5b00626
J. Phys. Chem. C 2015, 119, 9324−9333

system matrix effects are negligible for both helium and neon, then the I_A(Ne) vs I_A(He) and the I_B(Ne) vs I_B(He) curves are linear, as it was found for O/Cu(111). Along the same lines, the linearity of the I_{Cu}(Ne) vs I_{Cu}(He) curve and the nonlinearity of the I_{Ce}(Ne) vs I_{Ce}(He) curve indicated that the Ce(Ne) peak is affected by matrix effects, while the Cu(Ne) peak is not. Consequently, the latter peak can be used also for quantitative analysis as well. This approach is very useful for ternary systems, where the investigation of the I_A(Ne) vs I_B(Ne) curve can be meaningless because of the presence of the third element. It was applied to demonstrate the absence of neutralization effects for the Ce(Ne) peak upon CeO_2 deposition on Cu(111).[34]

For Co deposition on CeO_2(111), both the I_{Co}(Ne) vs I_{Co}(He) and the I_{Ce}(Ne) vs I_{Ce}(He) curves in Figure 2c,d, respectively, are close to linear, suggesting the absence of significant neutralization effects for the Co and Ce peaks for both He^+ and Ne^+. However, the evaporation of cobalt on the CeO_2(111) film induced a significant enhancement of the O(He) peak. Considering that the CeO_2(111) film is assumed to be oxygen-terminated, this strong increase is quite unexpected. For its understanding, it was useful to investigate with LEIS the adsorption of O_2 at 300 K on a thick, continuous Co film prepared on Cu(111) (Figure 3). Interestingly, with

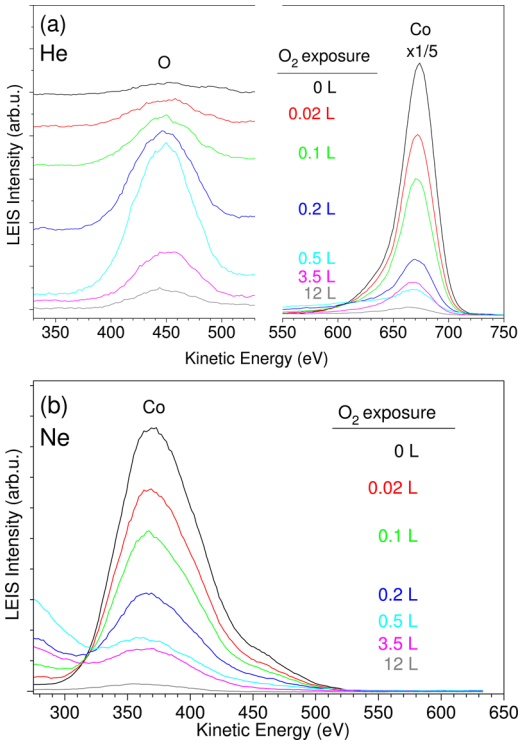

Figure 3. LEIS spectra obtained with helium (a) and neon (b) after exposition of a 16 ML thick Co film (on Cu(111)) to O_2 at 300 K. In (a), the Co region is attenuated by a factor of 5 with respect to the O region.

increasing O_2 exposure, the O(He) peak reached a maximum at ~0.5 L (1 L = 10^{-6} Torr × 1 s), and steeply decreased thereafter. The Co(He) and Co(Ne) peaks decreased monotonously with increasing O_2 exposure (Figure 3). The observed behavior clearly indicates a neutralization effect for the O peak. For this reason, the O LEIS peak was not used in our analysis of the Co/CeO_2(111) system. From the comparison of the Cu(He) and Co(He) LEIS peak areas of the clean Cu(111) surface and of the clean continuous Co film, a relative sensitivity factor for Co with respect to Cu was calculated: S_{Co} = 0.70. Please note that LEIS is much less sensitive for Ce; the relative sensitivity factor referenced to Cu under our experimental circumstances, using He, was 0.042.[34] Because of the high sensitivity of LEIS to Co, especially with He, the spectra of Figure 3a were collected with a much smaller ion flux compared to the other measurements in this paper.

The room temperature growth of Co on CeO_2(111) was investigated also by XPS (Figure 4). The Ce 3d region was monitored to characterize the oxidation state of the ceria film. The Ce 3d spectrum of the clean CeO_2(111) surface ("0 ML") is composed of three doublets (u‴, v‴), (u″, v″), and (u, v), corresponding to the emission from the spin−orbit split $3d_{3/2}$ and $3d_{5/2}$ core levels (Figure 4a).[51−53] The three doublets are assigned to different final states of tetravalent Ce (Ce^{4+} ions) in Ce compounds: u‴ (916.9 eV) and v‴ (898.6 eV) are due to a Ce $3d^94f^0$ O $2p^6$ final state, u″ (907.6 eV) and v″ (889.0 eV) to a Ce $3d^94f^1$ O $2p^5$ final state, and u (901.1 eV) and v (882.7 eV) to a Ce $3d^94f^2$ O $2p^4$ final state. The observed binding energies are in agreement with previous studies.[35,54] For a more detailed picture, which might allow a deeper understanding of the core levels and the properties of Ce in these spectra, we refer to ref 53. Note that, especially, the well separated u‴ peak at 916.9 eV is characteristic of the presence of Ce^{4+}.

Peak fitting revealed that the clean CeO_2(111) spectrum contained some contribution of reduced Ce^{3+} ions (Figure 5), which amounted to 5% of the total cerium intensity. The Ce 3d region of Ce_2O_3 consists of four peaks. They are assigned to two spin−orbit split doublets, (u′, v′) and (u_0, v_0), resulting from two different final states of Ce^{3+}. According to the literature, u′ (904.1 eV) and v′ (885.6 eV) are assigned to a Ce $3d^94f^1$ O $2p^6$ final state, and u_0 (899.8 eV) and v_0 (881.1 eV) to a Ce $3d^94f^2$ O $2p^5$ final state.[52] The deposition of Co at room temperature resulted in a well detectable growth of the reduced component, which is best visible as an intensity enhancement in the valleys at ~885.6 and ~904.1 eV (Figure 4a). The fraction of Ce^{3+} increased up to Θ_{Co} ~ 0.7 ML, and did not change considerably, when the amount of Co was further raised to 2.0 ML. This conclusion is supported by the peak fitting of the Ce 3d region presented in Figure 5. Note that, for the peak fitting, the binding energies and relative intensities of the Ce^{3+} and Ce^{4+} species were kept constant and only the intensities of the resulting two envelopes were allowed to vary. In accordance with previous results, an asymmetry for the u,v doublet for CeO_2 was allowed in the fitting.[54,55] The observed behavior clearly indicates an electron transfer from Co to ceria, especially at small coverages.

In accordance with this observation, a cationic character is expected for Co. In the literature data, for metallic cobalt (Co^0), an asymmetric Co $2p_{3/2}$ peak is observed at 778.0−778.5 eV. Co^{2+} is characterized by a Co $2p_{3/2}$ peak at 780−781 eV, with a strong satellite at 786−787 eV. The signature of Co^{3+} is a Co $2p_{3/2}$ peak at 780−781 eV with no satellite.[7,17,37,56,57] The deposition of 0.2 ML of Co on CeO_2(111) led to the appearance of the Co $2p_{3/2}$ peak at 781.0 eV and a strong satellite at 786.5 eV, assigned predominantly to Co^{2+} (Figure 4b). The doublet separation was ~16.0 eV, which fits very well with previous results on CoO.[58,59] Please note that the Co 2p doublet separation, which depends also on the spin state of the compound, can also be used for chemical identification.[58−60] For metallic Co and for

DOI: 10.1021/acs.jpcc.5b00626
J. Phys. Chem. C 2015, 119, 9324−9333

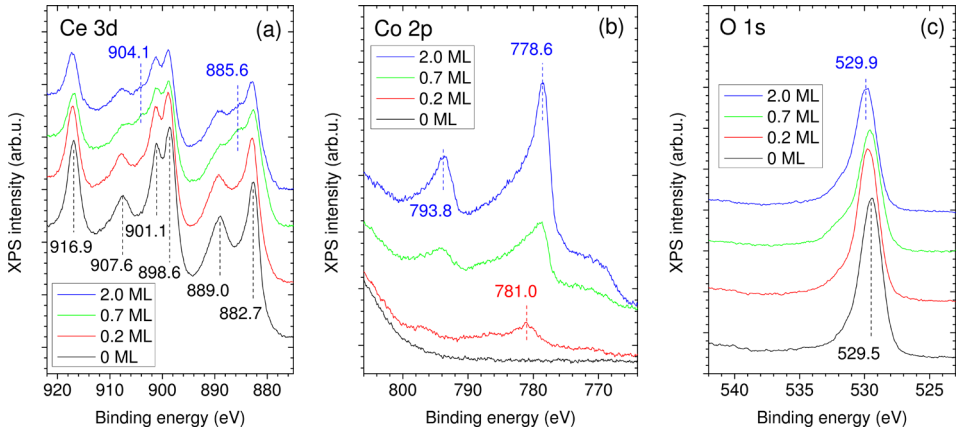

Figure 4. Ce 3d (a), Co 2p (b), and O 1s (c) regions of XPS spectra of the clean 16 ML CeO_2(111)/Cu(111) film and those collected after the deposition of different amounts of Co on top at 300 K.

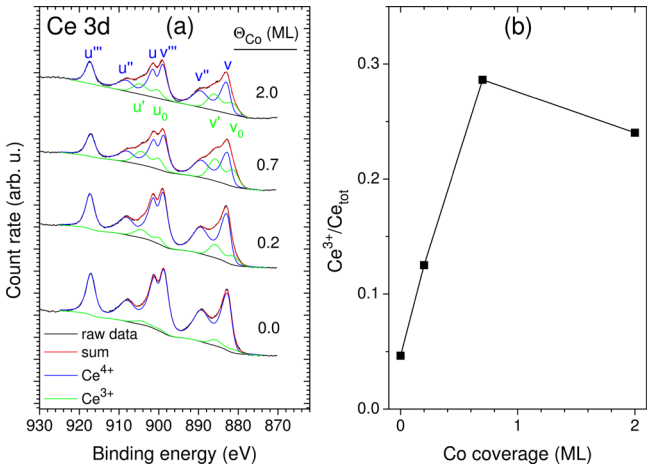

Figure 5. (a) Peak fitting for the Ce 3d spectra of the clean 16 ML CeO_2(111)/Cu(111) film and those collected after the deposition of different amounts of Co at 300 K. (b) The ratio of the Ce^{3+} XPS area and the total Ce area calculated from the fitting presented in (a).

Co^{3+}, the peak separation is ~15 eV. As the amount of cobalt was increased to 0.7 ML, the position of the Co $2p_{3/2}$ peak shifted to 779.0 eV, but it was very asymmetric toward higher binding energies and the satellite at 786.5 eV was still detectable. The surface at this point contained a mixture of Co^0 and Co^{2+}.

The cobalt deposit at Θ_{Co} = 2 ML was largely metallic, but very probably contained also a fraction of Co^{2+}. The broad feature at ~773 eV is assigned to the L_3VV Auger component of cobalt. A similar redox reaction between Co and ceria at room temperature was observed also by Martono et al.[37]

The Co (He) and Co (Ne) LEIS peak areas obtained after the deposition of 0.2 ML of Co on CeO_2(111) are only ~2% of those obtained on the continuous Co film, strongly indicating that oxygen diffusion from ceria to Co leads to a strong suppression of Co LEIS peaks already during Co deposition, and this process contributes significantly to the oxidation of Co observed by XPS. Nevertheless, Co LEIS peaks are still relatively strong (see the 300 K curves in Figure 6 a,d).

3.2. Thermal Characteristics of the Interaction of Co with CeO_2(111)/Cu(111). In the following, thermally induced changes of the Co deposits, investigated by LEIS and XPS, are presented. It is important to note that no dewetting of the CeO_2(111) film was observed up to 900 K by LEIS (not shown). In Figure 6, LEIS spectra obtained after Co deposition and subsequent stepwise annealing are presented for different Co coverages. In all cases, annealing led to an attenuation of the Co peak, accompanied by an increase of the Ce peak. At Θ_{Co} = 0.2 ML, the thermal treatment at 600 K resulted in a very strong (by 80%) decrease of the Co peaks monitored with both He^+ (Figure 6a) and Ne^+ (Figure 6d). The almost complete disappearance of the Co peak was observed at 800 K.

For the interpretation of these changes, it is useful to compare the LEIS spectra with the XPS data obtained in an analogous experiment (Figure 7). As mentioned above, at Θ_{Co} = 0.2 ML, exclusively Co^{2+} is formed upon deposition at 300 K, as evidenced by the Co $2p_{3/2}$ peak at 781.0 eV and its shake-up satellite at 786.6 eV (Figure 7b). The oxidation of cobalt is accompanied by the slight reduction in the Ce 3d region (Figure 7a). Subsequent annealing at higher temperatures did not change the oxidation state of cobalt. In contrast to LEIS measurements, the Co $2p_{3/2}$ peak only slightly decreased (by 10%) due to annealing at 600 K, and also, at 800 K, the Co 2p feature was well detectable, with 40% of the area observed at 300 K (cf. Figures 6a,d and 7b). On the basis of this comparison, desorption of Co from the surface can be excluded as the origin of the disappearance of Co contribution from LEIS spectra at 800 K. Similarly, agglomeration of oxidized Co particles on the surface cannot account for the complete suppression of the Co LEIS peaks. Hence, the observed behavior is assigned primarily to the diffusion of Co^{2+} ions into the ceria lattice. The slight reduction in the Ce 3d region observed upon Co deposition was reversed during annealing (Figure 7a), which can be rationalized by a redistribution of Ce^{3+} sites within the film: While reduced cerium ions initially form at the Co−ceria interface, at higher temperatures, an inward diffusion of Ce^{3+} ions and an outward diffusion of oxygen ions can take place. Note that a previous SIMS study indicated that self-diffusion in ceria is dominated by oxygen diffusion, while cerium cations are essentially immobile up to 900 K.[61] One might also argue that the thermal induced disappearance of Co LEIS peaks can be attributed to a further diffusion of oxygen from ceria to cobalt. There are two arguments against this assumption: (i) Although the adsorption of oxygen leads to a strong decrease in the Co peak, as shown in Figure 3, the Co LEIS peaks were easily detected. Moreover, it is not typical that the oxidation of a metal results in the complete disappearance of its LEIS peak.[49,62] A clear Co peak was detected also on Co_3O_4.[63] (ii) According to our XPS

DOI: 10.1021/acs.jpcc.5b00626
J. Phys. Chem. C 2015, 119, 9324−9333

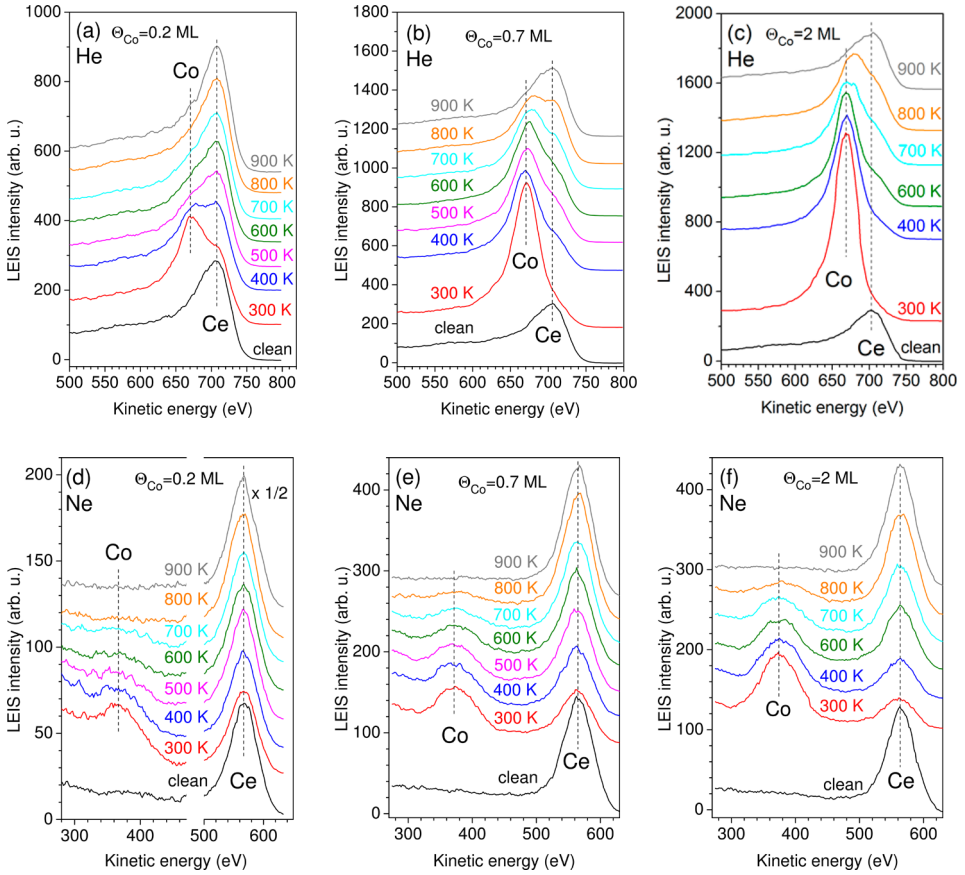

Figure 6. LEIS spectra obtained with He^+ (a–c) and Ne^+ (d–f) after the deposition of different amounts of Co on 16 ML CeO_2(111) at 300 K, followed by stepwise annealing for 5 min. The Ce peak in (d) is reduced by a factor of 2.

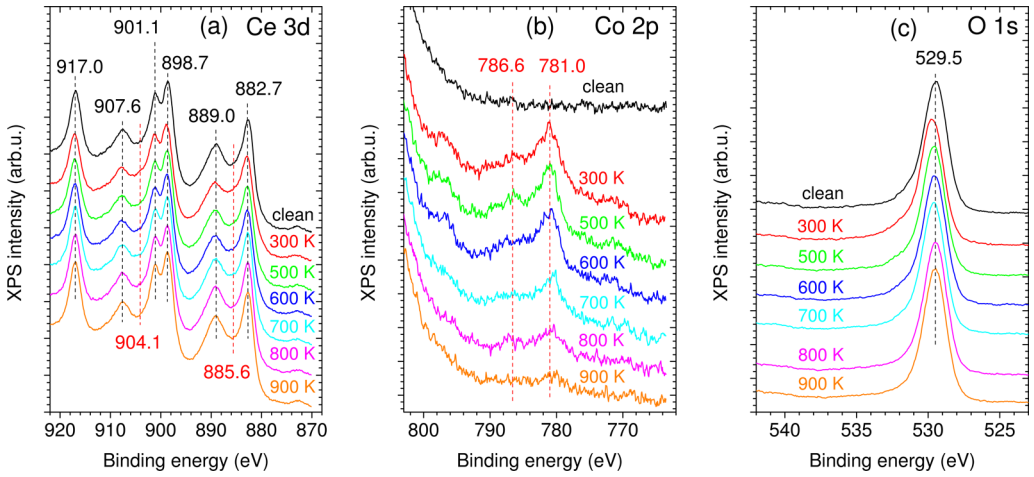

Figure 7. Ce 3d (a), Co 2p (b), and O 1s (c) regions of XPS spectra recorded after the deposition of 0.2 ML of Co on 16 ML CeO_2(111)/Cu(111) at 300 K, followed by subsequent annealing to higher temperature for 5 min. For comparison, the spectrum of the clean CeO_2(111) film is also displayed ("clean").

measurements, at a Co coverage of 0.2 ML, almost all Co atoms are oxidized to Co^{2+} during deposition. Annealing of this surface did not induce any appreciable changes in the Co 2p peak shape, suggesting that the disappearance of the Co LEIS peaks is not due to further oxidation of Co; therefore, we assign it to the diffusion of cobalt in the ceria film. It is worth to mention that this is not an example of Strong Metal Support Interaction (SMSI), because, in SMSI systems, *metallic* particles are buried by an overlayer of the support oxide.[21,49,64]

The LEIS annealing experiment for a higher Co coverage of Θ_{Co} = 0.7 ML yielded qualitatively similar results (Figure 6b,e). The main difference was that the attenuation of the Co peaks was less steep: both Co (He) and Co (Ne) intensities were relatively large at 600 K, and the complete suppression of the Co intensities occurred only at 900 K. XPS measurements proved that the deposition of 0.7 ML of Co at 300 K yielded a mixture of Co^0 and Co^{2+} (Figures 4b and 8b). Annealing up to 700 K led to a slight diminution of the overall Co $2p_{3/2}$

DOI: 10.1021/acs.jpcc.5b00626
J. Phys. Chem. C 2015, 119, 9324–9333

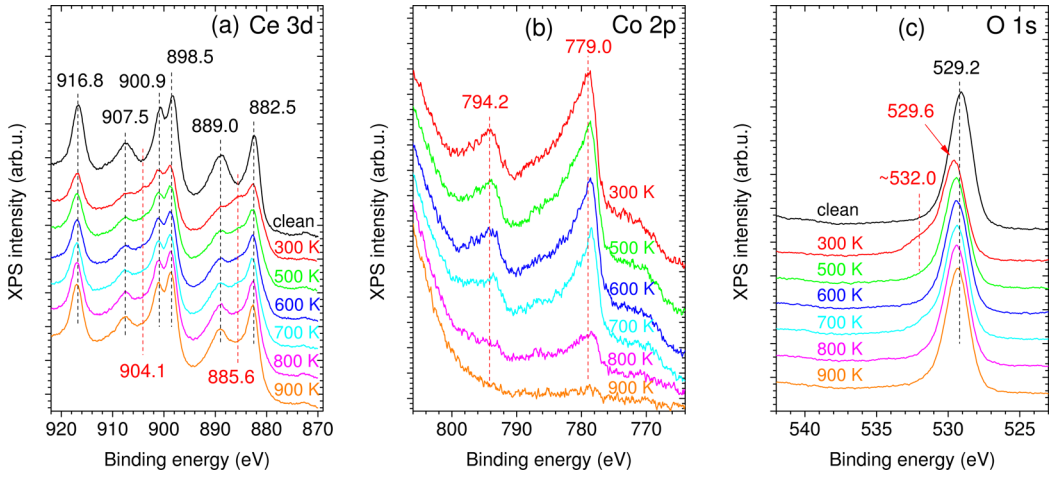

Figure 8. Ce 3d (a), Co 2p (b), and O 1s (c) regions of XPS spectra recorded after the deposition of 0.7 ML of Co on 16 ML $CeO_2(111)/Cu(111)$ at 300 K, followed by subsequent annealing to higher temperature for 5 min. For comparison, the spectrum of the clean $CeO_2(111)$ film is also displayed ("clean").

intensity. The peak became narrower and less asymmetric, due to a somewhat more metallic character, which indicates that Co^{2+} ions formed at room temperature can easily diffuse into the ceria film. Heating at 800 K resulted in a strong loss of cobalt intensity, and the broadening of the Co 2p feature toward higher binding energies implies a relative increase in the Co^{2+} component. After annealing at 900 K, the Co 2p doublet was barely detectable. In contrast to the behavior for Θ_{Co} = 0.2 ML, the metallic contribution to the Co 2p peak shape was significant at each temperature (Figure 8b). In the Ce 3d region, a reversal to the Ce^{4+} peak shape was observed upon annealing, which is primarily assigned to a redistribution of Ce^{3+} sites within the film.

Annealing of a 2 ML $Co/CeO_2(111)$ surface gave similar results with both LEIS (Figure 6c,f) and XPS (Figure 9a). The Co 2p region was dominated by the metallic component up to 700 K. At 800 K, a strong intensity loss and a broadening of the Co $2p_{3/2}$ peak was observed toward higher binding energies, and is assigned to a more oxidized character.

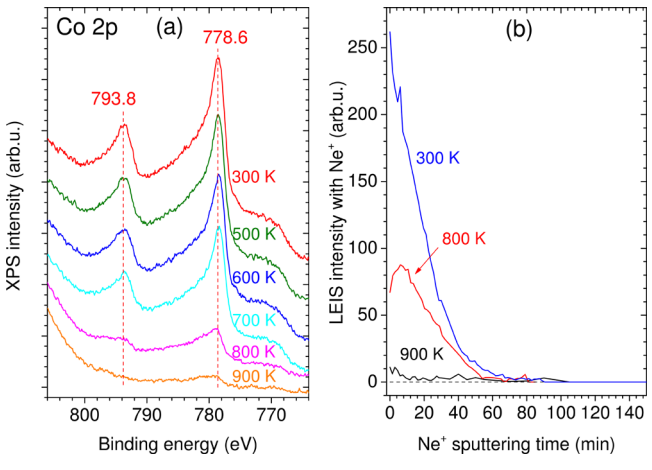

Figure 9. (a) Co 2p region of XPS spectra recorded after the deposition of 2 ML of Co on 16 ML $CeO_2(111)/Cu(111)$ at 300 K, followed by subsequent annealing to higher temperatures for 5 min. (b) Ne^+ sputter depth profiling performed at 300 K on 2 ML Co/16 ML $CeO_2(111)$ surfaces, which were prepared by evaporating 2 ML of Co on 16 ML $CeO_2(111)/Cu(111)$ at 300 K, followed by 5 min annealing at the given temperatures. The ion flux was ~120 nA/cm^2.

Since, at Θ_{Co} = 0.7 ML, and at 2 ML up to 700 K, the Co 2p peak contained a strong metallic contribution, and the growth mode of Co is of Volmer–Weber type, it is reasonable to assume that agglomeration of cobalt clusters also contributed to the observed attenuation of the Co LEIS intensities. On the other hand, since the diffusion of Co^{2+} into ceria was clearly proven for Θ_{Co} = 0.2 ML, it is expected that the oxidation of cobalt observed at $T \geq 800$ K for higher coverages is also accompanied by inward diffusion. In particular, the complete suppression of the Co LEIS peaks at 900 K can only be explained by this phenomenon (Figure 6). In order to obtain further proof for this process and to reveal additional details, Ne^+ ion depth profiling was performed for Θ_{Co} = 2 ML, after annealing the Co surface layer to different temperatures (Figure 9b).

The depth profiling of the 2 ML $Co/CeO_2(111)$ surface annealed to 900 K showed very small Co intensities in the whole sputtering period. Consequently, almost the whole amount of cobalt diffused through the ceria layer deep into the copper crystal at this temperature and was diluted there. Note that the Cu (Ne) signal appeared at a sputtering time of 90 min (not shown). The depth profiling performed right after Co deposition at 300 K reflected the gradual decrease in the Co intensity and its disappearance at ~70 min. The behavior observed after a 5 min annealing at 800 K was more complex: Initially, that is, in the first 8 min, an increase in the Co signal was found, indicating that the subsurface region of the ceria film is enriched in Co, which is attributed to the inward diffusion. Nevertheless, the Co (Ne) intensity was smaller in the whole sputtering period than in the "300 K" case, indicating that Co partly had already diffused into the copper crystal. Summarizing the information obtained from the depth profiling, there is a clear tendency for the migration of cobalt into ceria, but at higher temperatures, there is also a diffusion into the copper crystal underneath. Note that, in the previous XPS study of Martono et al., only agglomeration of Co was considered on ceria as an explanation for the increase in the Ce/Co signal ratio upon annealing.[37]

The influence of ceria stoichiometry on the growth and thermal properties of cobalt was also addressed. A reduced

DOI: 10.1021/acs.jpcc.5b00626
J. Phys. Chem. C 2015, 119, 9324–9333

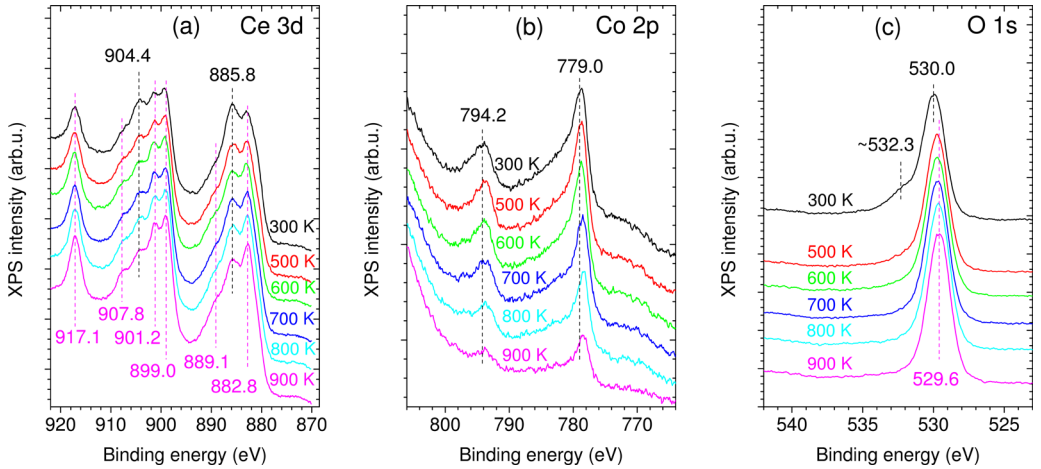

Figure 10. Deposition of 0.7 ML of Co on a reduced ceria surface at 300 K, followed by subsequent annealing, monitored by XPS. The reduced ceria surface was prepared by the deposition of 3 ML of metallic Ce on 12 ML $CeO_2(111)/Cu(111)$ at 523 K.

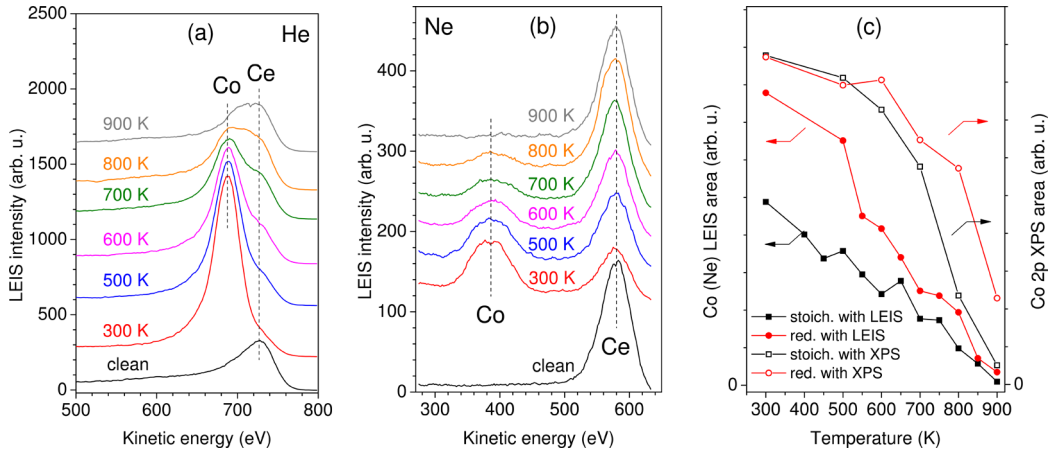

Figure 11. Deposition of 0.7 ML of Co on a reduced ceria surface at 300 K, followed by subsequent annealing monitored by LEIS with He^+ (a) and Ne^+ (b). The reduced ceria surface was prepared by the deposition of 3 ML of metallic Ce on 12 ML $CeO_2(111)/Cu(111)$ at 523 K (shown as "clean"). (c) Comparison of the Co (Ne) LEIS areas and the XPS areas of the Co $2p_{3/2}$ region (including the L_3VV Auger feature) obtained during annealing 0.7 ML of Co deposited on stoichiometric $CeO_2(111)$ and on reduced CeO_x surface.

CeO_x surface was prepared by evaporating 3 ML of metallic Ce at 523 K onto 12 ML $CeO_2(111)$ prepared on Cu(111). The Ce 3d region of this surface was dominated by the Ce^{3+} component, but Ce^{4+} was also present. When 0.7 ML of Co was deposited on this surface at 300 K, the Co $2p_{3/2}$ peak was narrower and somewhat less asymmetric than on $CeO_2(111)$ (Figure 10b). This line shape was assigned to a more metallic character, implying that the redox reaction between cobalt and ceria proceeds to a smaller extent on the reduced surface. The Co 2p region was dominated by the metallic peak shape in the whole temperature range (Figure 10b), in contrast to what was observed on $CeO_2(111)$ (Figure 8b). Moreover, the thermally induced attenuation of the Co 2p intensity was milder on the reduced ceria surface, suggesting that the inward diffusion of Co is more hindered. The latter statement was confirmed also by LEIS measurements (Figure 11a,b), which showed a less steep decrease in the Co peak on the reduced surface as a function of temperature. In the Ce 3d region, a slight reoxidation was observed, which is assigned to a homogenization of reduced Ce^{3+} ions within the film, which are initially preferentially located near the surface. A similar spectral change was observed in the Ce 3d region, also, during annealing, of the reduced ceria layer without Co (not shown).

In Figure 11c, the temperature dependence of the Co (Ne) LEIS areas and the Co 2p XPS areas (including the L_3VV Auger feature) obtained during annealing 0.7 ML of Co deposited on stoichiometric $CeO_2(111)$ and on the reduced CeO_x surface is presented. After Co deposition at 300 K, the Co LEIS area on the reduced surface was much higher than on the stoichiometric one. The origin of this difference can be twofold: (i) Smaller cobalt clusters may form on the reduced surface. This would be in agreement with previous studies indicating the formation of smaller gold clusters on reduced titanium oxide surfaces due to slower surface diffusion of Au atoms.[48,65] (ii) Alternatively, the extraction of oxygen from the ceria lattice by cobalt atoms proceeds to a lesser extent on the reduced surface, and consequently, the formed Co nanoparticles are less covered by oxygen.

At higher temperatures, the difference observed between Co LEIS areas on the two surfaces gets smaller, although the Co peak was always higher on reduced ceria. On the other hand, the difference in the Co XPS signal becomes stronger upon annealing (Figure 11c), indicating a less pronounced inward diffusion (a smaller average distance of Co atoms from the outermost surface) on reduced ceria after annealing. Since the Co 2p peak shape was largely metallic at 900 K, while the

DOI: 10.1021/acs.jpcc.5b00626
J. Phys. Chem. C 2015, 119, 9324−9333

almost complete disappearance of the Co LEIS peaks indicated the inward diffusion of Co, it is possible that an SMSI process (encapsulation) takes place on the reduced ceria.

4. SUMMARY AND CONCLUSIONS

We have investigated the interaction of cobalt with a continuous ultrathin $CeO_2(111)$ film by means of LEIS and XPS. The ceria layer was prepared on a Cu(111) single crystal using an established procedure by evaporation of Ce in an O_2 background. Co was deposited on this $CeO_2(111)$ film at room temperature by physical vapor deposition. From the LEIS measurements, a three-dimensional growth mode of Co was identified. It was verified that no disturbing neutralization effects occur for the Co peaks in LEIS; however, strong matrix effects are found for the O peak, which, therefore, was not used for quantitative analysis. At small coverages (Θ_{Co} = 0.2 ML), the whole amount of cobalt was oxidized to Co^{2+}; consequently, part of the ceria was reduced from Ce^{4+} to Ce^{3+}, as indicated by XPS. At higher coverages (Θ_{Co} = 0.7 and 2 ML), the XP spectra showed that an increasing fraction of Co remained in the metallic state, Co^0, after deposition. At higher temperatures, diffusion of Co^{2+} ions into the ceria film was found, and for Co^0, presumably also agglomeration takes place. At $T \geq 800$ K, extensive oxidation of the remaining Co atoms to Co^{2+} sets in, accompanied by diffusion into the ceria film. In this temperature range, also migration of a part of cobalt into the copper crystal occurs. Upon Co deposition on a reduced CeO_x surface, the redox reaction between cobalt and cerium was found to be much slower, which also led to a lower degree of cobalt migration into the cerium oxide film.

AUTHOR INFORMATION

Corresponding Author

*E-mail: ovari@chem.u-szeged.hu. Tel.: +36-62-343586. Fax: +36-62-544106. URL: http://www2.sci.u-szeged.hu/radio_rekin/indexrekin.htm (L.O.).

Notes

The authors declare no competing financial interest.

ACKNOWLEDGMENTS

This work was supported by the Alexander von Humboldt Foundation within the Research Group Linkage Program, by COST Action CM1104, and by the Cluster of Excellence "Engineering of Advanced Materials".

REFERENCES

(1) Trovarelli, A., Fornasiero, P., Eds. *Catalysis by Ceria and Related Materials*, 2nd ed.; Catalytic Science Series; Imperial College Press: London, 2013; Vol. *12*.

(2) Sun, C.; Li, H.; Chen, L. Nanostructured Ceria-Based Materials: Synthesis, Properties, and Applications. *Energy Environ. Sci.* **2012**, *5*, 8475.

(3) Trovarelli, A. Catalytic Properties of Ceria and CeO_2-Containing Materials. *Catal. Rev. Sci. Eng.* **1996**, *38*, 439−520.

(4) Park, S.; Vohs, J. M.; Gorte, R. J. Direct Oxidation of Hydrocarbons in a Solid-Oxide Fuel Cell. *Nature* **2000**, *404*, 265−267.

(5) Deluga, G. A.; Salge, J. R.; Schmidt, L. D.; Verykios, X. E. Renewable Hydrogen from Ethanol by Autothermal Reforming. *Science* **2004**, *303*, 993−997.

(6) Mattos, L. V.; Jacobs, G.; Davis, B. H.; Noronha, F. B. Production of Hydrogen from Ethanol: Review of Reaction Mechanism and Catalyst Deactivation. *Chem. Rev.* **2012**, *112*, 4094−4123.

(7) Óvári, L.; Krick Calderon, S.; Lykhach, Y.; Libuda, J.; Erdőhelyi, A.; Papp, C.; Kiss, J.; Steinrück, H.-P. Near Ambient Pressure XPS Investigation of the Interaction of Ethanol with $Co/CeO_2(111)$. *J. Catal.* **2013**, *307*, 132−139.

(8) Ferencz, Z.; Erdőhelyi, A.; Baán, K.; Oszkó, A.; Óvári, L.; Kónya, Z.; Papp, C.; Steinrück, H.-P.; Kiss, J. Effects of Support and Rh Additive on Co-Based Catalysts in the Ethanol Steam Reforming Reaction. *ACS Catal.* **2014**, *4*, 1205−1218.

(9) Varga, E.; Ferencz, Z.; Oszkó, A.; Erdőhelyi, A.; Kiss, J. Oxidation States of Active Catalytic Centers in Ethanol Steam Reforming Reaction on Ceria Based Rh Promoted Co Catalysts: An XPS Study. *J. Mol. Catal. A Chem.* **2015**, *397*, 127−133.

(10) Soykal, I. I.; Sohn, H.; Singh, D.; Miller, J. T.; Ozkan, U. S. Reduction Characteristics of Ceria under Ethanol Steam Reforming Conditions: Effect of the Particle Size. *ACS Catal.* **2014**, *4*, 585−592.

(11) Royer, S.; Duprez, D. Catalytic Oxidation of Carbon Monoxide over Transition Metal Oxides. *ChemCatChem* **2011**, *3*, 24−65.

(12) Llorca, J.; Homs, N.; Sales, J.; de la Piscina, P. R. Efficient Production of Hydrogen over Supported Cobalt Catalysts from Ethanol Steam Reforming. *J. Catal.* **2002**, *209*, 306−317.

(13) Lin, S. S.-Y.; Kim, D. H.; Ha, S. Y. Hydrogen Production from Ethanol Steam Reforming over Supported Cobalt Catalysts. *Catal. Lett.* **2008**, *122*, 295−301.

(14) Llorca, J.; Homs, N.; de la Piscina, P. R. In Situ DRIFT-Mass Spectrometry Study of the Ethanol Steam-Reforming Reaction over Carbonyl-Derived Co/ZnO Catalysts. *J. Catal.* **2004**, *227*, 556−560.

(15) Song, H.; Ozkan, U. S. The Role of Impregnation Medium on the Activity of Ceria-Supported Cobalt Catalysts for Ethanol Steam Reforming. *J. Mol. Catal. A Chem.* **2010**, *318*, 21−29.

(16) Bayram, B.; Soykal, I. I.; von Deak, D.; Miller, J. T.; Ozkan, U. S. Ethanol Steam Reforming over Co-Based Catalysts: Investigation of Cobalt Coordination Environment under Reaction Conditions. *J. Catal.* **2011**, *284*, 77−89.

(17) Hyman, M. P.; Vohs, J. M. Reaction of Ethanol on Oxidized and Metallic Cobalt Surfaces. *Surf. Sci.* **2011**, *605*, 383−389.

(18) Martono, E.; Hyman, M. P.; Vohs, J. M. Reaction Pathways for Ethanol on Model Co/ZnO(0001) Catalysts. *Phys. Chem. Chem. Phys.* **2011**, *13*, 9880−9886.

(19) Batista, M. S.; Santos, R. K. S.; Assaf, E. M.; Assaf, J. M.; Ticianelli, E. A. Characterization of the Activity and Stability of Supported Cobald Catalysts for the Steam Reforming of Ethanol. *J. Power Sources* **2003**, *124*, 99−103.

(20) Freund, H.-J. Clusters and Islands on Oxides: From Catalysis via Electronics and Magnetism to Optics. *Surf. Sci.* **2002**, *500*, 271−299.

(21) Diebold, U. The Surface Science of Titanium Dioxide. *Surf. Sci. Rep.* **2003**, *48*, 53−229.

(22) Fu, Q.; Wagner, T. Interaction of Nanostructured Metal Overlayers with Oxide Surfaces. *Surf. Sci. Rep.* **2007**, *62*, 431−498.

(23) Óvári, L.; Bugyi, L.; Majzik, Z.; Berkó, A.; Kiss, J. Surface Structure and Composition of Au−Rh Bimetallic Nanoclusters on $TiO_2(110)$: A LEIS and STM Study. *J. Phys. Chem. C* **2008**, *112*, 18011−18016.

(24) Óvári, L.; Berkó, A.; Balázs, N.; Majzik, Z.; Kiss, J. Formation of Rh−Au Core−Shell Nanoparticles on $TiO_2(110)$ Surface Studied by STM and LEIS. *Langmuir* **2010**, *26*, 2167−2175.

(25) Berkó, A.; Balázs, N.; Kassab, G.; Óvári, L. Segregation of K and Its Effects on the Growth, Decoration, and Adsorption Properties of Rh Nanoparticles on $TiO_2(110)$. *J. Catal.* **2012**, *289*, 179−189.

(26) Mullins, D. R.; Radulovic, P. V.; Overbury, S. H. Ordered Cerium Oxide Thin Films Grown on Ru(0001) and Ni(111). *Surf. Sci.* **1999**, *429*, 186−198.

(27) Lu, J.-L.; Gao, H.-J.; Shaikhutdinov, S.; Freund, H.-J. Morphology and Defect Structure of the CeO_2(1 1 1) Films Grown on Ru(0 0 0 1) as Studied by Scanning Tunneling Microscopy. *Surf. Sci.* **2006**, *600*, 5004−5010.

(28) Siokou, A.; Nix, R. M. Interaction of Methanol with Well-Defined Ceria Surfaces: Reflection/Absorption Infrared Spectroscopy, X-ray Photoelectron Spectroscopy, and Temperature-Programmed Desorption Study. *J. Phys. Chem. B* **1999**, *103*, 6984−6997.

DOI: 10.1021/acs.jpcc.5b00626
J. Phys. Chem. C 2015, 119, 9324−9333

(29) Matolín, V.; Libra, J.; Matolínová, I.; Nehasil, V.; Sedláček, L.; Šutara, F. Growth of Ultra-Thin Cerium Oxide Layers on Cu(111). *Appl. Surf. Sci.* **2007**, *254*, 153−155.
(30) Šutara, F.; Cabala, M.; Sedláček, L.; Skála, T.; Škoda, M.; Matolín, V.; Prince, K. C.; Cháb, V. Epitaxial Growth of Continuous CeO_2(111) Ultra-Thin Films on Cu(111). *Thin Solid Films* **2008**, *516*, 6120−6124.
(31) Staudt, T.; Lykhach, Y.; Tsud, N.; Skála, T.; Prince, K. C.; Matolín, V.; Libuda, J. Ceria Reoxidation by CO_2: A Model Study. *J. Catal.* **2010**, *275*, 181−185.
(32) Dvořák, F.; Stetsovych, O.; Steger, M.; Cherradi, E.; Matolínová, I.; Tsud, N.; Škoda, M.; Skála, T.; Mysliveček, J.; Matolín, V. Adjusting Morphology and Surface Reduction of CeO_2(111) Thin Films on Cu(111). *J. Phys. Chem. C* **2011**, *115*, 7496−7503.
(33) Rodriguez, J. A.; Graciani, J.; Evans, J.; Park, J. B.; Yang, F.; Stacchiola, D.; Senanayake, S. D.; Ma, S.; Pérez, M.; Liu, P.; et al. Water-Gas Shift Reaction on a Highly Active Inverse CeOx/Cu(111) Catalyst: Unique Role of Ceria Nanoparticles. *Angew. Chem., Int. Ed.* **2009**, *48*, 8047−8050.
(34) Vári, G.; Óvári, L.; Kiss, J.; Kónya, Z. LEIS and XPS Investigation into the Growth of Cerium and Cerium Dioxide on Cu(111). *Phys. Chem. Chem. Phys.* **2015**, *17*, 5124−5132.
(35) Alexandrou, M.; Nix, R. M. The Growth, Structure and Stability of Ceria Overlayers on Pd(111). *Surf. Sci.* **1994**, *321*, 47−57.
(36) Weast, R. C., Astle, M. J., Eds. *CRC Handbook of Chemistry and Physics*, 60th ed.; CRC Press: Boca Raton, FL, 1979.
(37) Martono, E.; Vohs, J. M. Support Effects in Cobalt-Based Ethanol Steam Reforming Catalysts: Reaction of Ethanol on Co/CeO_2/YSZ(100) Model Catalysts. *J. Catal.* **2012**, *291*, 79−86.
(38) Zhou, J.; Baddorf, A. P.; Mullins, D. R.; Overbury, S. H. Growth and Characterization of Rh and Pd Nanoparticles on Oxidized and Reduced CeOx(111) Thin Films by Scanning Tunneling Microscopy. *J. Phys. Chem. C* **2008**, *112*, 9336−9345.
(39) Lu, J. L.; Gao, H. J.; Shaikhutdinov, S.; Freund, H. J. Gold Supported on Well-Ordered Ceria Films: Nucleation, Growth and Morphology in CO Oxidation Reaction. *Catal. Lett.* **2007**, *114*, 8−16.
(40) Hyman, M. P.; Martono, E.; Vohs, J. M. Studies of the Structure and Interfacial Chemistry of Co Layers on ZnO(0001). *J. Phys. Chem. C* **2010**, *114*, 16892−16899.
(41) Dumont, J.; Mugumaoderha, C. M.; Seldrum, T.; Frising, F.; Moisson, C.; Turover, D.; Sporken, R. Formation of (Zn,Co)O by Annealing of Co Overlayers on ZnO. *J. Vac. Sci. Technol., B: Microelectron. Nanometer Struct.* **2007**, *25*, 1536.
(42) Napetschnig, E.; Schmid, M.; Varga, P. Pd, Co and Co-Pd Clusters on the Ordered Alumina Film on NiAl(1 1 0): Contact Angle, Surface Structure and Composition. *Surf. Sci.* **2007**, *601*, 3233−3245.
(43) Shao, Y.; Chen, W.; Wold, E.; Paul, J. Dispersion and Electronic Structure of TiO_2-Supported Cobalt and Cobalt Oxide. *Langmuir* **1994**, *10*, 178−187.
(44) Brongersma, H. H.; Draxler, M.; de Ridder, M.; Bauer, P. Surface Composition Analysis by Low-Energy Ion Scattering. *Surf. Sci. Rep.* **2007**, *62*, 63−109.
(45) Shirley, D. A. High-Resolution X-ray Photoemission Spectrum of the Valence Bands of Gold. *Phys. Rev. B* **1972**, *5*, 4709−4714.
(46) Napetschnig, E.; Schmid, M.; Varga, P. Growth of Ce on Rh(111). *Surf. Sci.* **2004**, *556*, 1−10.
(47) Staudt, T.; Lykhach, Y.; Hammer, L.; Schneider, M. A.; Matolín, V.; Libuda, J. A Route to Continuous Ultra-Thin Cerium Oxide Films on Cu(111). *Surf. Sci.* **2009**, *603*, 3382−3388.
(48) Parker, S. C.; Grant, A. W.; Bondzie, V. A.; Campbell, C. T. Island Growth Kinetics during the Vapor Deposition of Gold onto TiO_2(110). *Surf. Sci.* **1999**, *441*, 10−20.
(49) Pesty, F.; Steinrück, H.-P.; Madey, T. E. Thermal Stability of Pt Films on TiO_2(110): Evidence for Encapsulation. *Surf. Sci.* **1995**, *339*, 83−95.
(50) Kürnsteiner, P.; Steinberger, R.; Primetzhofer, D.; Goebl, D.; Wagner, T.; Druckmüllerova, Z.; Zeppenfeld, P.; Bauer, P. Matrix Effects in the Neutralization of He Ions at a Metal Surface Containing Oxygen. *Surf. Sci.* **2013**, *609*, 167−171.
(51) Fujimori, A. Correlation Effects in the Electronic Structure and Photoemission Spectra of Mixed-Valence Cerium Compounds. *Phys. Rev. B* **1983**, *28*, 4489−4499.
(52) Pfau, A.; Schierbaum, K. D. The Electronic Structure of Stoichiometric and Reduced CeO_2 Surfaces: An XPS, UPS and HREELS Study. *Surf. Sci.* **1994**, *321*, 71−80.
(53) Nelin, C. J.; Bagus, P. S.; Ilton, E. S.; Chambers, S. A.; Kuhlenbeck, H.; Freund, H.-J. Relationships between Complex Core Level Spectra and Materials Properties. *Int. J. Quantum Chem.* **2010**, *110*, 2752−2764.
(54) Engelhard, M.; Azad, S.; Peden, C. H. F.; Thevuthasan, S. X-ray Photoelectron Spectroscopy Studies of Oxidized and Reduced CeO_2(111) Surfaces. *Surf. Sci. Spectra* **2004**, *11*, 73.
(55) Skála, T.; Šutara, F.; Prince, K. C.; Matolín, V. Cerium Oxide Stoichiometry Alteration via Sn Deposition: Influence of Temperature. *J. Electron Spectrosc. Relat. Phenom.* **2009**, *169*, 20−25.
(56) Wagner, C. D.; Riggs, W. M.; Davis, L. E.; Moulder, J. F. *Handbook of X-Ray Photoelectron Spectroscopy*; Muilenberg, G. E., Ed.; Perkin-Elmer Corporation: Eden Praire, MN, 1979.
(57) Lin, S. S. Y.; Kim, D. H.; Engelhard, M. H.; Ha, S. Y. Water-Induced Formation of Cobalt Oxides over Supported Cobalt/Ceria-Zirconia Catalysts under Ethanol-Steam Conditions. *J. Catal.* **2010**, *273*, 229−235.
(58) Chuang, T. J.; Brundle, C. R.; Rice, D. W. Interpretation of the X-ray Photoemission Spectra of Cobalt Oxides and Cobalt Oxide Surfaces. *Surf. Sci.* **1976**, *59*, 413−429.
(59) Schenck, C. V.; Dillard, J. G.; Murray, J. W. Surface Analysis and the Adsorption of Co(II) on Goethite. *J. Colloid Interface Sci.* **1983**, *95*, 398−409.
(60) Schmid, M.; Kaftan, A.; Steinrück, H.-P.; Gottfried, J. M. The Electronic Structure of Cobalt(II) Phthalocyanine Adsorbed on Ag(111). *Surf. Sci.* **2012**, *606*, 945−949.
(61) Perkins, C. L.; Henderson, M. A.; Peden, C. H. F.; Herman, G. S. Self-Diffusion in Ceria. *J. Vac. Sci. Technol., A* **2001**, *19*, 1942.
(62) Jacobs, J.-P.; Reijne, S.; Elfrink, R. J. M.; Mikhailov, S. N.; Brongersma, H. H. Quantification of the Composition of Alloy and Oxide Surfaces Using Low-Energy Ion Scattering. *J. Vac. Sci. Technol., A* **1994**, *12*, 2308−2313.
(63) Carson, G. A.; Nassir, M. H.; Langell, M. A. Epitaxial Growth of Co_3O_4 on CoO(100). *J. Vac. Sci. Technol., A* **1996**, *14*, 1637−1642.
(64) Óvári, L.; Kiss, J. Growth of Rh Nanoclusters on TiO_2(1 1 0): XPS and LEIS Studies. *Appl. Surf. Sci.* **2006**, *252*, 8624−8629.
(65) Sedona, F.; Sambi, M.; Artiglia, L.; Rizzi, G. A.; Vittadini, A.; Fortunelli, A.; Granozzi, G. Mobility of Au on TiO_x Substrates with Different Stoichiometry and Defectivity. *J. Phys. Chem. C* **2008**, *112*, 3187−3190.

DOI: 10.1021/acs.jpcc.5b00626
J. Phys. Chem. C 2015, 119, 9324−9333